



UNIVERSITY OF LEEDS

This is a repository copy of *Temperature and Pressure Dependent Kinetics of QOOH Decomposition and Reaction with O₂: Experimental and Theoretical Investigations of QOOH Radicals Derived from Cl + (CH₃)₃COOH*.

White Rose Research Online URL for this paper:
<http://eprints.whiterose.ac.uk/152873/>

Version: Accepted Version

Article:

Whelan, CA, Blitz, MA orcid.org/0000-0001-6710-4021, Shannon, R et al. (4 more authors) (2019) Temperature and Pressure Dependent Kinetics of QOOH Decomposition and Reaction with O₂: Experimental and Theoretical Investigations of QOOH Radicals Derived from Cl + (CH₃)₃COOH. *The Journal of Physical Chemistry A*, 123 (47). [acs.jpca.9b08785](https://doi.org/10.1021/acs.jpca.9b08785). pp. 10254-10262. ISSN 1089-5639

<https://doi.org/10.1021/acs.jpca.9b08785>

© 2019 American Chemical Society. This is an author produced version of a journal article published in *Journal of Physical Chemistry A*. Uploaded in accordance with the publisher's self-archiving policy.

Reuse

Items deposited in White Rose Research Online are protected by copyright, with all rights reserved unless indicated otherwise. They may be downloaded and/or printed for private study, or other acts as permitted by national copyright laws. The publisher or other rights holders may allow further reproduction and re-use of the full text version. This is indicated by the licence information on the White Rose Research Online record for the item.

Takedown

If you consider content in White Rose Research Online to be in breach of UK law, please notify us by emailing eprints@whiterose.ac.uk including the URL of the record and the reason for the withdrawal request.



eprints@whiterose.ac.uk
<https://eprints.whiterose.ac.uk/>

Temperature and Pressure Dependent Kinetics of QOOH Decomposition and Reaction with O₂: Experimental and Theoretical Investigations of QOOH Radicals Derived from Cl + (CH₃)₃COOH

Charlotte A. Whelan, Mark A. Blitz,* Robin Shannon, Lavinia Onel, James P. Lockhart, Paul W. Seakins, Daniel Stone*

School of Chemistry, University of Leeds, Leeds, LS2 9JT, UK

* Corresponding authors

Abstract

QOOH radicals are key species in autoignition, produced by internal isomerisations of RO₂ radicals, and are central to chain branching reactions in low temperature combustion. The kinetics of QOOH radical decomposition and reaction with O₂ have been determined as a function of temperature and pressure, using observations of OH radical production and decay following H-atom abstraction from tertiary-butyl hydroperoxide ((CH₃)₃COOH) by Cl atoms to produce QOOH (\cdot CH₂(CH₃)₂COOH) radicals. The kinetics of QOOH decomposition have been investigated as a function of temperature (251 to 298 K), and pressure (10 to 350 Torr), in helium and nitrogen bath gases, and those of the reaction between QOOH and O₂ have been investigated as a function of temperature (251 to 304 K), and pressure (10 to 100 Torr) in He and N₂. Decomposition of the QOOH radicals was observed to display temperature and pressure dependence, with a barrier height for decomposition of (44.7 ± 4.0) kJ mol⁻¹ determined by master equation fitting to the experimental data. The rate coefficient for the reaction between QOOH and O₂ was determined to be $(5.6 \pm 1.7) \times 10^{-13}$ cm³ s⁻¹ at 298 K, with no significant dependence on pressure, and can be described by the Arrhenius parameters $A = (7.3 \pm 6.8) \times 10^{-14}$ cm³ s⁻¹ and $E_a = -(5.4 \pm 2.1)$ kJ mol⁻¹ in the temperature range 251 to 304 K. This work represents the first measurements of any QOOH radical kinetics as a function of temperature and pressure.

Introduction

Fuel chemistry plays a central role in autoignition processes and low temperature combustion strategies designed to lower NO_x (NO_x = NO + NO₂) emissions and soot formation. This chemistry

is key to the development and efficient use of alternative fuels, and is dominated by reactions involving QOOH carbon-centred radicals.^{1,2}

Fuel consumption in low temperature combustion and autoignition (summarised in Figure 1) is initiated through hydrogen-abstraction reactions, resulting in generation of radicals, R, which undergo association reactions with O₂ to produce peroxy radicals, RO₂. Isomerisation reactions of RO₂ radicals, involving internal H-atom shifts, produce carbon-centred hydroperoxy radicals, QOOH, which dictate the balance between propagation and branching of the radical chain reactions. Decomposition of QOOH, producing a cyclic ether and an OH radical for alkyl hydroperoxy radicals, propagates the radical chain reactions. In competition with QOOH decomposition, addition of O₂ to the QOOH radical centre leads to the production of O₂QOOH, the decomposition of which generate a ketohydroperoxide and OH. The subsequent decomposition of the ketohydroperoxide to produce further OH gives rise to chain branching. Chain branching is the pivotal process in autoignition, and QOOH radical chemistry is thus of fundamental importance in fuel combustion. In addition, the impact of auto-oxidation processes involving gas phase QOOH radicals in atmospheric oxidation processes on the formation of highly oxygenated molecules (HOMs) and aerosol particles is receiving increasing recognition.³

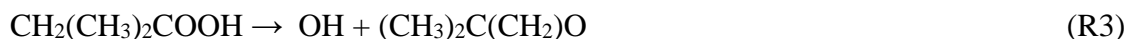
Despite the significance of QOOH radicals, direct measurements of QOOH species and their kinetics are extremely limited. While there have been several observations of reaction products resulting from QOOH chemistry,⁴⁻⁶ there has been only a single report of direct QOOH observations, in which a resonance stabilised QOOH species produced from 1,3-cycloheptadiene was detected using multiplexed photoionisation mass spectrometry (MPIMS) with tunable vacuum ultraviolet (VUV) synchrotron radiation.⁷ The challenges associated with direct QOOH detection arise from low steady state QOOH concentrations owing to stabilisation of RO₂ radicals in deep energy minima (typically $-(125 - 150)$ kJ mol⁻¹ with respect to R + O₂ and $-(45 - 70)$ kJ mol⁻¹ with respect to QOOH) at low temperatures, while at higher temperatures increased QOOH production rates are offset by rapid removal reactions.¹ Figure 2 shows a typical potential energy surface (PES) for the production of RO₂ and QOOH following R + O₂, demonstrating that low QOOH concentrations arise from the relative thermodynamic stability of RO₂ and the likely rapid removal of any QOOH formed through decomposition to OH as well as reactions involving O₂. Until recently, chemical models of combustion and autoignition have relied on indirect evidence and high-level theoretical calculations to predict the reactivity and behaviour of QOOH and O₂QOOH radicals.¹

Zádor et al.⁸ reported the first direct measurements of any QOOH reaction kinetics. Critically, Zádor et al. were able to produce the $\cdot\text{CH}_2(\text{CH}_3)_2\text{COOH}$ (2-hydroperoxy-2-methylprop-1-yl) QOOH radical

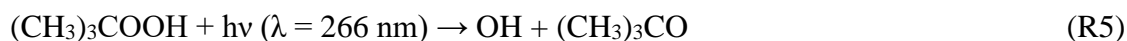
directly via abstraction of hydrogen from the C-H bonds in t-butyl hydroperoxide ((CH₃)₃COOH) by chlorine atoms (R1-R2a):



Rates of QOOH radical decomposition (R3) and reaction with O₂ (R4) were determined using infrared absorption spectroscopy to monitor the production of OH radicals:



While production of OH was observed through photolysis of (CH₃)₃COOH (R5),⁹ the photolytic production occurred on a much shorter timescale than that through R3, enabling separation of the timescale of OH production from QOOH loss (R3 and R4) from the photolytic process:



Loss of OH from the system occurs through reaction with (CH₃)₃COOH (R6), which, in contrast to the H-atom abstraction by Cl, has been indicated by experiment⁹ and theory¹⁰ to occur exclusively at the O-H bond:⁸



Infrared absorption measurements of OH by Zádor et al.⁸ thus enabled determination of the kinetics of QOOH decomposition (R3) and QOOH + O₂ (R4), and the first direct kinetic measurements for any QOOH species. Moreover, experiments using the MPIMS technique were also able to identify the cyclic ether ((CH₃)₂C(CH₂)O, 2,2-dimethyloxirane, DMO) product of the QOOH decomposition (R3), and daughter ions of the O₂QOOH (O₂CH₂(CH₃)₂COOH) product of QOOH + O₂ (R4).

The unimolecular decomposition of QOOH (R3) was shown to be pressure dependent over the range 8 – 90 Torr in He at room temperature, with a combination of experimental data and high-level calculations giving k_3^0 (298 K) = $5.89 \times 10^{-13} \text{ cm}^3 \text{ s}^{-1}$, k_3^∞ (298 K) = $4.80 \times 10^4 \text{ s}^{-1}$ and $F_c = 0.544$ in He, with a dissociation barrier of 48.1 kJ mol⁻¹ (11.5 kcal mol⁻¹). The reaction between QOOH and O₂ (R4) was shown to be independent of pressure in the range 4 – 90 Torr He, with the MPIMS experiments at 4 Torr giving $k_4 = 1.1 \times 10^{-12} \text{ cm}^3 \text{ s}^{-1}$ and the OH absorption experiments between 8 and 90 Torr giving $k_4 = 8.5 \times 10^{-13} \text{ cm}^3 \text{ s}^{-1}$. Combination of the results from the two techniques gave $k_4 = (9.0 \pm 3.0) \times 10^{-13} \text{ cm}^3 \text{ s}^{-1}$ at 298 K. Theoretical investigation of the PES for the system indicated

barrierless production of O₂QOOH in R4, with stabilisation of the O₂QOOH species resulting in no further radical production under the experimental conditions as the internal abstraction required before radical production has a significant energy barrier, making the O₂QOOH stable at 300 K, in agreement with calculations for other similar systems.¹¹

In this work, we report an investigation of the temperature and pressure dependence of the kinetics of QOOH decomposition (R3) and of the reaction of QOOH with O₂ (R4) for the QOOH radical derived from Cl + (CH₃)₃COOH (R2), using laser-induced fluorescence (LIF) spectroscopy to monitor the OH radical production in the system. Results are reported for experiments conducted at temperatures between 251 and 304 K and pressures in the range 10-350 Torr. Treatment of the reaction system using the Master Equation Solver for Multi-Energy Well Reactions (MESMER)¹² is also reported, and is used to place the experimental results in context.

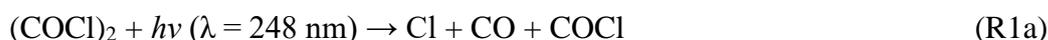
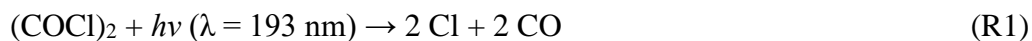
Experimental

Experiments were conducted in a slow-flow reactor described in a number of previous publications.¹³⁻¹⁵ Reactions were initiated by laser flash photolysis and monitored using laser-induced fluorescence (LIF) spectroscopy of OH reaction products. Precursor gas mixtures ((CH₃)₃COOH/(COCl)₂/He/O₂ or (CH₃)₃COOH/(COCl)₂/N₂/O₂) were prepared in a gas manifold and passed into a stainless steel six-way cross reactor at known flow rates regulated by calibrated mass flow controllers. The reactor was welded into a metal bath, with only the ends of the reactor arms protruding through the walls of the bath. The total pressure in the reactor, monitored by a capacitance manometer, was controlled by a needle valve on the exhaust line to the pumps. The bath was filled with methanol which was cooled to the desired temperature by a refrigerated immersion probe (LabPlant Refrigerated Immersion Probe, RP-100CD), enabling control of sub-ambient reaction temperatures. Temperatures in the reactor were measured by K-type thermocouples situated close to the reaction zone.

A known flow of carrier gas (He or N₂) was passed through a bubbler containing degassed t-butylhydroperoxide ((CH₃)₃COOH) (Sigma Aldrich, 70 % v/v aqueous) to entrain (CH₃)₃COOH into the precursor gas flow. Oxalyl chloride ((COCl)₂, Sigma Aldrich ≥ 99 %) was prepared at a known concentration in He or N₂ and stored in a glass bulb. He (BOC, 99.99 %), N₂ (BOC, oxygen free, 99.99 %) and O₂ (BOC, 99.999 %) were used as supplied.

Reactions were initiated by pulsed excimer laser (Lambda Physik Compex) photolysis of (COCl)₂ at 193 nm (typical fluence < 1 mJ cm⁻²) or 248 nm (typical fluence 10-30 mJ cm⁻²). At a wavelength of 193 nm, photolysis of (COCl)₂ produces 2 Cl + 2 CO directly (R1), while at 248 nm the photolysis

produces Cl + CO + COCl (R1a), which is followed by decomposition of the COCl fragment to produce CO + Cl (R1b):¹⁶



The photolysis laser beam was introduced into the reactor through one of the side arms, with the majority of the experiments performed at a pulse repetition frequency of 10 Hz, although experiments were conducted at lower repetition frequencies to ensure that there were no interferences from photolysis of reaction products.

QOOH ($\text{CH}_2(\text{CH}_3)_2\text{COOH}$) radicals were generated by the reaction of Cl atoms with $(\text{CH}_3)_3\text{COOH}$ (R2a), with production of RO_2 radicals ($(\text{CH}_3)_3\text{CO}_2$, R2b) through abstraction of the peroxide H-atom not contributing to observed kinetics in this work.



OH radicals, produced in the system by decomposition of QOOH radicals (R3) and photolysis of $(\text{CH}_3)_3\text{COOH}$ (R5), were monitored by off-resonance laser-induced fluorescence (LIF) following excitation at 282 nm ($\text{A}^2\Sigma (v'=1) \leftarrow \text{X}^2\Pi (v''=0), \text{Q}_1(1)$).



Laser light at 282 nm was generated using the 532 nm output of an Nd:YAG (Continuum Powerlite 8010) to pump a dye laser (Spectra Physics PDL-3) operating on Rhodamine-6-G dye. The off-resonant OH fluorescence at ~ 308 nm, passed through an interference filter (Barr Associates, 308 ± 5 nm), was detected by a photomultiplier (Electron tube 9813 QB) mounted perpendicular to the plane of the photolysis and probe laser beams. The photomultiplier signal was digitized and integrated by an oscilloscope (LeCroy LT262), and passed to a computer for data analysis. The time delay between photolysis and probe laser pulses was controlled by a homebuilt digital delay generator based on National Instruments hardware and varied to enable monitoring of the OH profile as a function of time following photolysis of the gas mixture. Kinetic traces, examples of which are shown in Figure 3, typically consisted of 200 time points, with each time point averaged 5-10 times.

Experiments were performed at each temperature over a range of pressures (10 – 350 Torr) and concentrations of O₂ ($3.9 \times 10^{15} - 1.7 \times 10^{17} \text{ cm}^{-3}$). Precursor concentrations were also varied in the ranges $9.0 \times 10^{13} - 4.0 \times 10^{16} \text{ cm}^{-3}$ for (CH₃)₃COOH and $4.5 \times 10^{13} - 5.0 \times 10^{15} \text{ cm}^{-3}$ for (COCl)₂.

Analysis

The temporal profiles of OH in the system are governed by reactions R1-R6 and can be described by the analytical expression given by Equation 1:

$$S_{\text{OH}}(t) = S_0 \exp(-k_{1b}[M]t) + S_1 \exp(-k'_2 t) + S_2 \exp(-(k_3 + k'_4) t) + S_3 \exp(-k'_6 t)$$

(Equation 1)

where S_{OH}(t) is the observed OH signal and coefficients S₀, S₁, S₂ and S₃ are linked to the production of OH through R1b, R2, R3 and R5, respectively. The coefficient S₀ is equal to zero for photolysis at experiments at 193 nm. The rate coefficient k_{1b} is that for the decomposition of COCl, which is constrained in the analysis to previous measurements,¹⁷ k'₂ is the pseudo-first-order rate coefficient for R2 (i.e. k'₂ = k₂[(CH₃)₃COOH]), k₃ is the rate coefficient for QOOH decomposition (R3), k'₄ is the pseudo-first-order rate coefficient for R4 (k'₄ = k₄[O₂]) since O₂ is in large excess over QOOH, and k'₆ is the pseudo-first-order rate coefficient describing the loss of OH from the system, which, although strictly includes any loss of OH through diffusion, is approximated here as being dominated by R6 (such that k'₆ = k₆[(CH₃)₃COOH]).

The kinetic parameters k₃ and k₄ were determined by global fitting Equation 1 to the observed OH LIF signals. Typically, five or more temporal profiles obtained at similar temperatures ($\pm 2 \text{ K}$) and pressures ($\pm 2 \text{ Torr}$) with different concentrations of (CH₃)₃COOH (and thus different values for k'₂ and k'₆ but equal values for k₂ and k₆) were fitted globally to find a single common value for k₃ (obtained in the absence of O₂) or k₄ (in the presence of O₂, constraining k₃ to values determined in the absence of O₂). Experiments were performed to measure k₄ using both 193 nm and 248 nm photolysis under otherwise identical conditions, with no significant differences observed between the results.

The time constant for chemical production of OH gives information on the pseudo-first-order loss process of QOOH (k₃ + k₄[O₂]), but in addition, the ratio of prompt to reactive OH obtained through the coefficients S₂ and S₃ provides information on k₃:k₄. As additional oxygen is added, a smaller fraction of QOOH decomposes and the OH production associated with R3, and hence S₂, decreases.

The additional decrease in the overall fluorescence signal owing to fluorescence quenching associated with O₂ collisions can be accounted for by the change in the prompt OH signal, which is given by S₃, with [O₂]. The analysis presented in this work using the analytical expression (Equation 1) considers not only the time dependence of the OH fluorescence signal as a function of [O₂], but also the ratio of prompt and reactive OH signal. Further details are given in the Supporting Information.

In order to optimise the sensitivity of the fits to k₃ and k₄, conditions were employed such that the formation of QOOH through reaction R2 was rapid compared to its subsequent decay through reactions R3 and R4, requiring high concentrations of (CH₃)₃COOH. Owing to the use of aqueous (CH₃)₃COOH in this study and the similarity in vapour pressures between water and (CH₃)₃COOH,⁹ the peroxide concentrations were approximated from the vapour pressure and flow rates in the system, assuming that the peroxide contributed 55 % of the total (CH₃)₃COOH/H₂O vapour pressure in keeping with the work of Baasandorj et al.⁹ Independent experiments were performed in the absence of (COCl)₂ and O₂ (i.e. using (CH₃)₃COOH/He or (CH₃)₃COOH/N₂ gas mixtures) to determine the pseudo-first-order loss rate coefficients k'₆ (k'₆ = k₆[(CH₃)₃COOH]) for a range of (CH₃)₃COOH concentrations at a given temperature and pressure and to verify that the resulting bimolecular rate coefficients k₆ determined were in agreement with those reported by Baasandorj et al.⁹

Fits to the experimental observations gave uncertainties in individual rate coefficients on the order of 5 %. While it was possible to minimise the effects of correlations between fit parameters by employing conditions to optimise the sensitivity to the kinetic parameters of interest, it was not possible to avoid correlations entirely. Uncertainties quoted for k₃ were thus determined from fits in which other kinetic parameters were fixed to ± 50 % of their values determined from global fits in which all relevant kinetic parameters were treated as variables, and are on the order of 30 %. Uncertainties reported for k₄ were determined in a similar manner and include the uncertainties associated with k₃.

Results and Discussion

QOOH (CH₂(CH₃)₂COOH) Decomposition Kinetics

Figure 3 shows typical OH fluorescence signals following initiation of chemistry within the system. Photolysis of (CH₃)₃COOH results in the instantaneous OH production observed at t = 0, with the subsequent growth in OH, in the absence of O₂, associated solely with QOOH decomposition. The initial abstraction reaction generating QOOH (R2a) is close to thermoneutral (~ -4 kJ mol⁻¹)¹⁸, hence it is expected that the decomposition of QOOH is entirely thermal, with no contribution from

chemical activation. No evidence was observed in the fits to OH to suggest any influence from chemically activated processes. QOOH decomposition kinetics (k_3) were thus determined from global fits of data obtained in experiments performed in the absence of O₂ to Equation 1. Figure 4 shows k_3 as a function of temperature and pressure, with the experimental data given in Table 1. The results at 298 K in He bath gas are in general agreement with the behaviour observed by Zádor et al., although the results obtained in this work are systematically lower than those reported previously by ~30-40 %. Results at 298 K in N₂ bath gas show faster decomposition kinetics as expected for a pressure dependent reaction, owing to the greater efficiency of collisional energy transfer in N₂ compared to He.

The fits to Equation 1 also give the pseudo-first-order rate coefficients k'_2 , which describes the kinetics of QOOH formation from Cl + (CH₃)₃COOH (R2), and k'_6 , which describes the kinetics of OH loss through OH + (CH₃)₃COOH (R6). Although the concentration of (CH₃)₃COOH is only approximated from the vapour pressure and flow rates in the system, results for k'_2 and k'_6 can be used with the approximate (CH₃)₃COOH concentrations to approximate the bimolecular rate coefficients k_2 and k_6 .

Results for k_2 indicate a value of $(2.4 \pm 0.7) \times 10^{-11} \text{ cm}^3 \text{ s}^{-1}$ at 298 K and a temperature dependence described by $k_2 = (2.3 \pm 2.1) \times 10^{-12} \exp[(690 \pm 250)/T] \text{ cm}^3 \text{ s}^{-1}$ over the conditions investigated in this work. The value for k_2 determined in this work using the approximate concentration of (CH₃)₃COOH is significantly lower than the value of $7.7 \times 10^{-11} \text{ cm}^3 \text{ s}^{-1}$ used in the analysis performed by Zádor et al.,⁸ which was based on the kinetics and branching ratio for the reaction between Cl and (CH₃)₃CH¹⁹. A lower value for k_2 , as determined in this work, is supported by the similar measured value of $(3.15 \pm 0.24) \times 10^{-11} \text{ cm}^3 \text{ s}^{-1}$ for Cl + (CH₃)₃COH.²⁰ The ratio of k_2 to k_6 determined in this work, which is independent of the absolute concentration of (CH₃)₃COOH, was (10.7 ± 4.8) at 298 K. Using $k_6 = (3.58 \pm 0.54) \times 10^{-12} \text{ cm}^3 \text{ s}^{-1}$ at 296 K as reported by Baasandorj et al.,⁹ the observed $k_2:k_6$ ratio indicates a value for k_2 of $(3.8 \pm 1.7) \times 10^{-11} \text{ cm}^3 \text{ s}^{-1}$, which is also significantly lower than that adopted in the analysis performed by Zádor et al. Fits to Equation 1 in which k_2 was fixed to a value of $7.7 \times 10^{-11} \text{ cm}^3 \text{ s}^{-1}$ gave values for k_3 that were 5-10 % higher than those in which k_2 was allowed to float, which may explain some of the difference in results between this work and that of Zádor et al. shown in Figure 3.

At 298 K, this work indicates $k_6 = (2.2 \pm 0.7) \times 10^{-12} \text{ cm}^3 \text{ s}^{-1}$, with a temperature dependence described by $k_6 = (1.0 \pm 0.7) \times 10^{-13} \exp[(890 \pm 210)/T] \text{ cm}^3 \text{ s}^{-1}$. The results of Baasandorj et al. gave $k_6 = (7.0 \pm 1.0) \times 10^{-13} \exp[(485 \pm 20)/T] \text{ cm}^3 \text{ s}^{-1}$ obtained in experiments using pulsed laser photolysis of (CH₃)₃COOH at 248 nm coupled to OH detection via LIF. Reaction R6 has the potential to interfere with the chemistry, as abstraction from the methyl groups in (CH₃)₃COOH would lead to the

generation of QOOH and hence OH regeneration, with the results that the growth and decay of OH could then no longer be simply associated with reactions R3, R4, R6 and diffusional OH loss. While the standard experiments performed by Baasandorj et al. would be insensitive to fast OH regeneration from R3, in several experiments Baasandorj et al. added high concentrations of O₂ ($(2-4) \times 10^{16} \text{ cm}^{-3}$) to intercept any QOOH formed before decomposition to OH, and observed no change in the measured bimolecular rate coefficient, concluding that H-atom abstraction from the methyl groups of the molecule was insignificant. Our analysis is based on (CH₃)₃CO₂ being the sole product of R6, consistent with theory¹⁰ and with the experimental evidence which does not indicate any growth of OH from the photolysis of (CH₃)₃COOH. In this scenario the observed decay of OH following production from the decomposition of QOOH is associated with R6 and diffusional loss and should not vary with the concentration of O₂. No significant change in the rate coefficient describing the OH loss in the system (k'_6) as a function of the O₂ concentration was observed in this work (see Supporting Information for further details), indicating that the loss of OH is independent of O₂ and that (CH₃)₃CO₂ is the sole product of R6. Further details and results for k_2 , k_6 , and the effects of the concentration of O₂ on k'_6 are provided in the Supporting Information.

Master Equation Analysis

Statistical rate theory calculations were performed to describe the decomposition kinetics of QOOH using the master equation simulation package Master Equation Solver for Multi-Energy well Reactions (MESMER), which has been described in detail in previous work.¹²

The geometries, vibrational frequencies and rotational constants for the QOOH species and its transition state to decomposition were calculated at the M06-2X/cc-pVTZ level of theory using the Gaussian 09 suite of programs²¹ using the geometries reported by Zádor et al.⁸ as inputs. Hindered rotation potentials were obtained from M06-2X/6-31+G** relaxed scans along the various dihedral co-ordinates in both the well and the transition state. Hindered rotor state densities were obtained using the methodology within MESMER which has been described previously.²² Pressure dependent rate coefficients were calculated using MESMER utilising a rigid rotor-harmonic oscillator approximation for all apart from the hindered modes, which were assumed to be separable. Collisional energy transfer within the system was described by an exponential down model with the average energy transferred in a downward direction on collision with the bath gas represented by $\langle \Delta E \rangle_{\text{down}}$. All Lennard Jones parameters used to describe collisions with the bath gas were obtained from the Joback method²³ as implemented in the Reaction Mechanism Generator (RMG) described by Gao et al.²⁴ An input file for the MESMER calculations is provided in the Supporting Information.

Given the extensive experimental dataset both $\langle\Delta E\rangle_{\text{down}}$ and the barrier height to decomposition were varied in order to fit the master equation to the experimental rate coefficients. To this end, a Levenburg-Marquardt algorithm, as implemented in MESMER, was used to minimise the merit function:

$$\chi^2 = \sum_i \frac{(k_{\text{exp}}(p_i, T_i) - k_{\text{mod}}(p_i, T_i))^2}{\sigma_i^2}$$

(Equation 2)

where $k_{\text{exp}}(p_i, T_i)$ and $k_{\text{mod}}(p_i, T_i)$ are the experimental and modelled rate coefficients at pressure p_i and temperature T_i , respectively, with σ_i^2 representing the appropriate experimental uncertainty, which is based on the measured uncertainties and is assumed to scale linearly with the magnitude of the rate coefficient.

Figure 4 shows the fit to the experimental data, which gave a barrier height to decomposition of 44.7 kJ mol⁻¹, $\langle\Delta E\rangle_{\text{down}} = 89$ cm⁻¹ in He, and $\langle\Delta E\rangle_{\text{down}} = 147$ cm⁻¹ in N₂. The barrier height reported in this work is lower than the value of 52.3 kJ mol⁻¹ (12.5 kcal mol⁻¹) value determined from the high level calculations (QCISD(T)/CBS//M06-2X/6-311++G(d,p)) reported by Zádor et al. Typical uncertainties in the high level calculations are approximately ± 4 kJ mol⁻¹ (1 kcal mol⁻¹),⁸ but Zádor et al. also required a reduction in the barrier height to 48.1 kJ mol⁻¹ (11.5 kcal mol⁻¹) to give a better fit with their experimental data at 298 K when using $\langle\Delta E\rangle_{\text{down}} = 250$ cm⁻¹. In addition, Zádor et al. noted that the value for $\langle\Delta E\rangle_{\text{down}}$ was poorly constrained, with a lower value correlating with a lower barrier height. While there is a slight inconsistency between the fitted and calculated barrier heights, there are potentially several contributing factors, and the difference reported here is significantly less than in our recent study on CH₂OCH₂OOH decomposition.¹¹

Simulations in MESMER constrained to the barrier height and $\langle\Delta E\rangle_{\text{down}}$ reported by Zádor et al. tend to underestimate the observed values for k_3 reported in this work and those by Zádor et al. (see Supporting Information for further details). However, fitting the results of Zádor et al. using MESMER gave poorly defined results when both the barrier height and $\langle\Delta E\rangle_{\text{down}}$ were varied together owing to correlations between the parameters which are difficult to characterise using data obtained at a single temperature. Fits to the results of Zádor et al. in which the barrier height was constrained to 48.1 kJ mol⁻¹ required a value for $\langle\Delta E\rangle_{\text{down}}$ in excess of 650 cm⁻¹, while fits constrained to the barrier of 44.7 kJ mol⁻¹ determined in this work gave an optimum $\langle\Delta E\rangle_{\text{down}}$ of 94 cm⁻¹. Conversely, fits constrained to $\langle\Delta E\rangle_{\text{down}} = 250$ cm⁻¹ used in the work of Zádor et al. gave an optimum barrier height of 47.1 kJ mol⁻¹, while fits constrained to $\langle\Delta E\rangle_{\text{down}} = 89$ cm⁻¹, as determined in this

work, gave an optimum barrier height of 44.8 kJ mol⁻¹. Results are summarised in the Supporting Information. Results reported in this work are constrained to both the pressure and temperature dependence of the decomposition and thus provide greater opportunity to define both the barrier to decomposition, which was determined to be 44.7 kJ mol⁻¹, and the collisional energy transfer parameter $\langle\Delta E\rangle_{\text{down}}$, which was determined to be 89 cm⁻¹ in He and 147 cm⁻¹ in N₂.

The optimised values for the barrier height and $\langle\Delta E\rangle_{\text{down}}$ were used in MESMER simulations to determine k_3 at temperatures between 200 and 800 K and pressures between 1 and 10⁶ Torr in He and N₂. The calculated rate coefficients were parameterised using the Troe expression for broad falloff curves²⁵ (Equations 3-6) for use in kinetic models to assess the competition between chain propagation and chain branching reactions:

$$k = \frac{k_0[M]k_\infty}{k_0[M] + k_\infty} F \quad (\text{Equation 3})$$

$$F = \frac{\left(1 + k_0[M]/k_\infty\right)}{\left(1 + \left(k_0[M]/k_\infty\right)^n\right)^{1/n}} \quad (\text{Equation 4})$$

$$n = \left(\frac{\ln(2)}{\ln(2/F_c)}\right) \left((1 - b) + b \left(k_0[M]/k_\infty\right)^q\right) \quad (\text{Equation 5})$$

$$q = \frac{(F_c - 1)}{\ln(F_c/10)} \quad (\text{Equation 6})$$

where $k_{3,0}(T)$ is the low-pressure and $k_{3,\infty}(T)$ is the high-pressure limiting rate coefficient for QOOH decomposition, M is the total number density, and F_c is the broadening factor. The fits to the MESMER output for k_3 (shown in the Supporting Information) give $k_{3,0} = 3.27 \times 10^{-7} (T/298)^{-6.675} \exp(-4746/T) \text{ cm}^3 \text{ s}^{-1}$, $k_{3,\infty} = 1.57 \times 10^{13} (T/298)^{0.344} \exp(-5457/T) \text{ s}^{-1}$, $F_c = 0.212$ and $b = 0.213$ in He

bath gas and $k_{3,0} = 6.06 \times 10^{-6} (T/298)^{-6.649} \exp(-4762/T) \text{ cm}^3 \text{ s}^{-1}$, $k_{3,\infty} = 1.54 \times 10^{13} (T/298)^{0.355} \exp(-5452/T) \text{ s}^{-1}$, $F_c = 0.206$ and $b = 0.215$ in N_2 .

QOOH ($\text{CH}_2(\text{CH}_3)_2\text{COOH}$) + O_2 Kinetics

Figure 3 shows temporal profiles for OH recorded in the presence of varying amounts of O_2 . In the presence of O_2 , the yield of OH produced via QOOH decomposition is reduced owing to competition between the decomposition process and $\text{QOOH} + \text{O}_2$ (R4), and the rate of the non-photolytic production of OH is increased owing to the increased rate of QOOH consumption. Measurements were made at pressures between 10 and 100 Torr at temperatures between 251 and 304 K to determine k_4 , the rate coefficient for O_2 addition to QOOH. Fits to Equation 1 were performed with kinetics for R1-3 constrained to the values reported above for each temperature and pressure, with k_4 determined from the pseudo-first-order rate coefficient k'_4 ($k'_4 = k_4[\text{O}_2]$). Values for k_4 determined from fits in which k_4 was treated as a global parameter at each temperature, with the O_2 concentration constrained for each experiment, were typically within 10 % of those obtained from fits in which k'_4 ($k'_4 = k_4[\text{O}_2]$) was treated as a local parameter for each experiment, with results at one temperature (282 K) within 25 % and associated with larger uncertainties (see Supporting Information for further details).

At 298 K, results from this work indicate $k_4 = (5.6 \pm 1.7) \times 10^{-13} \text{ cm}^3 \text{ s}^{-1}$, compared to the previous measurement⁸ of $(9.0 \pm 3.0) \times 10^{-13} \text{ cm}^3 \text{ s}^{-1}$ and the calculated value of $12.5 \times 10^{-13} \text{ cm}^3 \text{ s}^{-1}$.⁸ Owing to the complexity of the mechanism controlling OH in the system, the sensitivity of the fits to k_4 was investigated by performing fits to the data in which k_4 was fixed to a range of values while k_2 and k_6 were allowed to float. The variation in χ^2 for fits performed with different fixed values of k_4 for temperatures between 251 and 298 K indicate that, at each temperature, the minimum in the χ^2 , which indicates the best fit to the data, corresponds to the value of k_4 determined by the unconstrained fits to Equation 1, giving confidence in the results for k_4 . However, it can also be observed that k_4 is better defined at low temperatures than at 298 K, with fits at lower temperatures displaying a steeper change in χ^2 around the minimum value than the fit at 298 K.

No significant dependence of k_4 on pressure was observed, consistent with the results of Zádor et al. over the range of 4 – 90 Torr He at room temperature, and with other measurements of $\text{R} + \text{O}_2$ reactions, where, for $>\text{C}_3$ alkyl radicals, the reactions appear to be at their high pressure limits at similar pressures at room temperature.²⁶ Effects of pressure were investigated in the range 10-100 Torr at 298 K, with fits to individual pressures giving $k_4 = (4.9 \pm 1.5) \times 10^{-13} \text{ cm}^3 \text{ s}^{-1}$ at 10 Torr, $k_4 = (6.4 \pm 2.2) \times 10^{-13} \text{ cm}^3 \text{ s}^{-1}$ at 60 Torr, and $k_4 = (5.5 \pm 2.1) \times 10^{-13} \text{ cm}^3 \text{ s}^{-1}$ at 100 Torr. Experiments

were also performed at 298 K using photolysis wavelengths of 193 nm and 248 nm, under otherwise identical conditions, to assess the impact of the production and subsequent decomposition of COCl (R1a and R1b) on the observed kinetics. For experiments at 193 nm, the S_0 term in Equation 1 is equal to zero, while for those experiments performed at 248 nm the S_0 term is included, with k_{1b} constrained to the previous measurements of Ghosh et al.¹⁷ No significant differences were observed between values for k_4 determined from experiments using 193 nm photolysis ($k_4 = (5.3 \pm 1.7) \times 10^{-13} \text{ cm}^3 \text{ s}^{-1}$) compared to those using 248 nm ($k_4 = (5.5 \pm 2.1) \times 10^{-13} \text{ cm}^3 \text{ s}^{-1}$). The result given for k_4 of $(5.6 \pm 1.7) \times 10^{-13} \text{ cm}^3 \text{ s}^{-1}$ at 298 K is the average of all experiments at this temperature.

Figure 5 shows the temperature dependence of k_4 , which can be described by the Arrhenius parameters $A = (7.3 \pm 6.8) \times 10^{-14} \text{ cm}^3 \text{ s}^{-1}$ and $E_a = -(5.4 \pm 2.1) \text{ kJ mol}^{-1}$. Results are summarised in Table 2. The observed behaviour is consistent with that that expected for a barrierless potential energy surface for the reaction between $\text{CH}_2(\text{CH}_3)_2\text{COOH}$ and O_2 as predicted by the calculations of Zádor et al.

The rate coefficient for the reaction of the QOOH species investigated in this work with O_2 at 298 K is significantly larger than the value of $(2.9 \pm 1.0) \times 10^{-15} \text{ cm}^3 \text{ s}^{-1}$ observed at 10 Torr and 400 K for the resonance stabilised QOOH species produced in the oxidation of 1,3-cycloheptadiene.⁷ Such differences have been attributed to the stability of the QOOH species derived from 1,3-cycloheptadiene, which is enhanced by allylic resonance stabilisation, and highlight that $\text{QOOH} + \text{O}_2$ kinetics may vary significantly from one QOOH species to another. Rate coefficients for $\text{QOOH} + \text{O}_2$ reactions used in models of combustion chemistry are often estimated from $\text{R} + \text{O}_2$ reactions on the basis that both reaction types involve addition of O_2 to a carbon-centred radical.^{1,2} For the QOOH species investigated in this work, the rate coefficient for $\text{QOOH} + \text{O}_2$ is less than that for the analogous $\text{R} + \text{O}_2$ reaction by a factor of ~ 10 .²⁷⁻³⁰ In contrast, the rate coefficient for $\text{QOOH} + \text{O}_2$ for the QOOH species derived from 1,3-cycloheptadiene was shown to be greater than that for the analogous $\text{R} + \text{O}_2$ by a factor of ~ 10 .⁷ The use of $\text{R} + \text{O}_2$ kinetics to estimate $\text{QOOH} + \text{O}_2$ reaction rates may therefore require greater consideration of the effects of any resonance stabilisation and more detailed examination of the relevant potential energy surfaces.

Conclusions

Observations of OH radical production and decay following H-atom abstraction from $(\text{CH}_3)_3\text{COOH}$ by Cl atoms to produce QOOH ($\text{CH}_2(\text{CH}_3)_2\text{COOH}$) radicals have been used to determine the kinetics of QOOH decomposition and the reaction between QOOH and O_2 as a function of temperature and pressure. The decomposition of QOOH radicals was observed to display pressure dependence between 10 and 350 Torr. Master equation analysis, using MESMER, was used to investigate the decomposition reaction and to fit the barrier height for decomposition to the experimental data, yielding a barrier height of $(44.7 \pm 4.0) \text{ kJ mol}^{-1}$, compared to a value of 52.3 kJ mol^{-1} determined previously by high level calculations,⁸ and collisional energy transfer parameters of $\langle \Delta E \rangle_{\text{down}} = 89 \text{ cm}^{-1}$ in He bath gas and $\langle \Delta E \rangle_{\text{down}} = 147 \text{ cm}^{-1}$ in N_2 bath gas. The rate coefficient for the reaction between QOOH and O_2 was determined to be $(5.6 \pm 0.5) \times 10^{-13} \text{ cm}^3 \text{ s}^{-1}$ at 298 K, and was shown to be independent of pressure in the range 10 to 100 Torr. Kinetics of $\text{QOOH} + \text{O}_2$ were also investigated as a function of temperature between 251 and 304 K, and can be described by the Arrhenius parameters $A = (7.3 \pm 6.8) \times 10^{-14} \text{ cm}^3 \text{ s}^{-1}$ and $E_a = -(5.4 \pm 2.1) \text{ kJ mol}^{-1}$.

Supporting Information

Further details regarding the determination of kinetics parameters from fits to the observed OH time profiles, and sensitivity of the fits, are provided in the supporting information. The MESMER input file used in the analysis is also provided. This material is available free of charge via the Internet at <http://pubs.acs.org>.

Author Information

Corresponding Authors

D. Stone (d.stone@leeds.ac.uk) and M.A. Blitz (m.blitz@leeds.ac.uk)

Notes

The authors declare no competing financial interest.

Acknowledgements

CAW thanks the Engineering and Physical Sciences Research Council for a studentship. The authors are also grateful to the Engineering and Physical Sciences Research Council (EPSRC, grant reference EP/J010871/1) and the Natural Environment Research Council (NERC, grant reference NE/L010798/1) for funding.

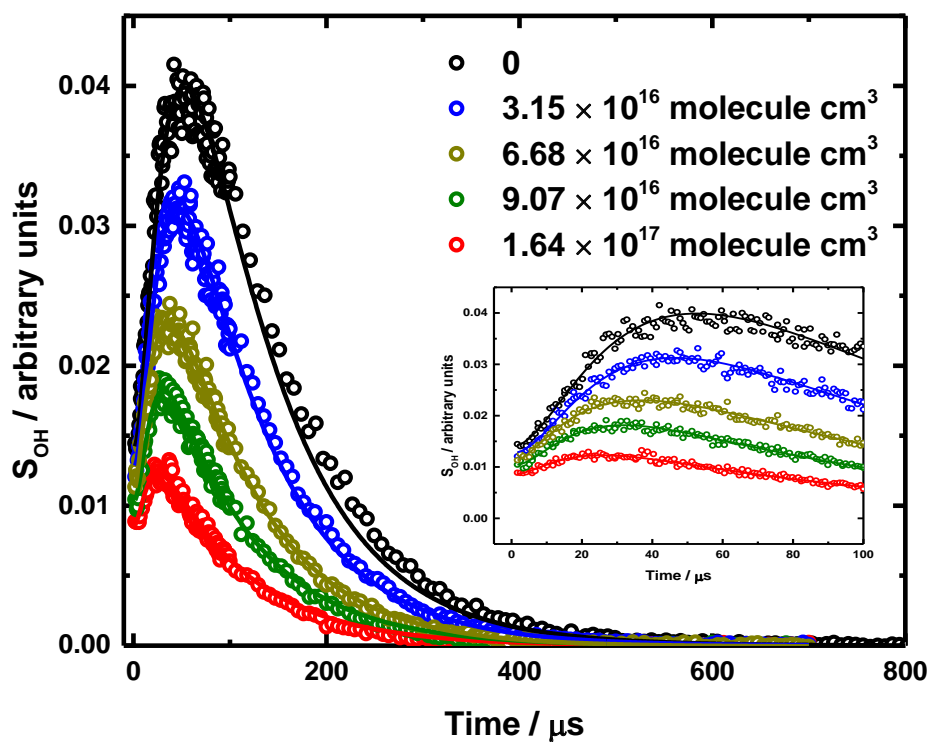


Figure 3: Typical OH fluorescence signals (S_{OH}) (10 Torr N_2 , 298 K) for a range of O_2 concentrations (0 cm^{-3} (black); $3.15 \times 10^{16} \text{ cm}^{-3}$ (blue); $6.68 \times 10^{16} \text{ cm}^{-3}$ (brown); $9.07 \times 10^{16} \text{ cm}^{-3}$ (green); $1.64 \times 10^{16} \text{ cm}^{-3}$ (red)). The inset shows the first 100 μs in greater detail.

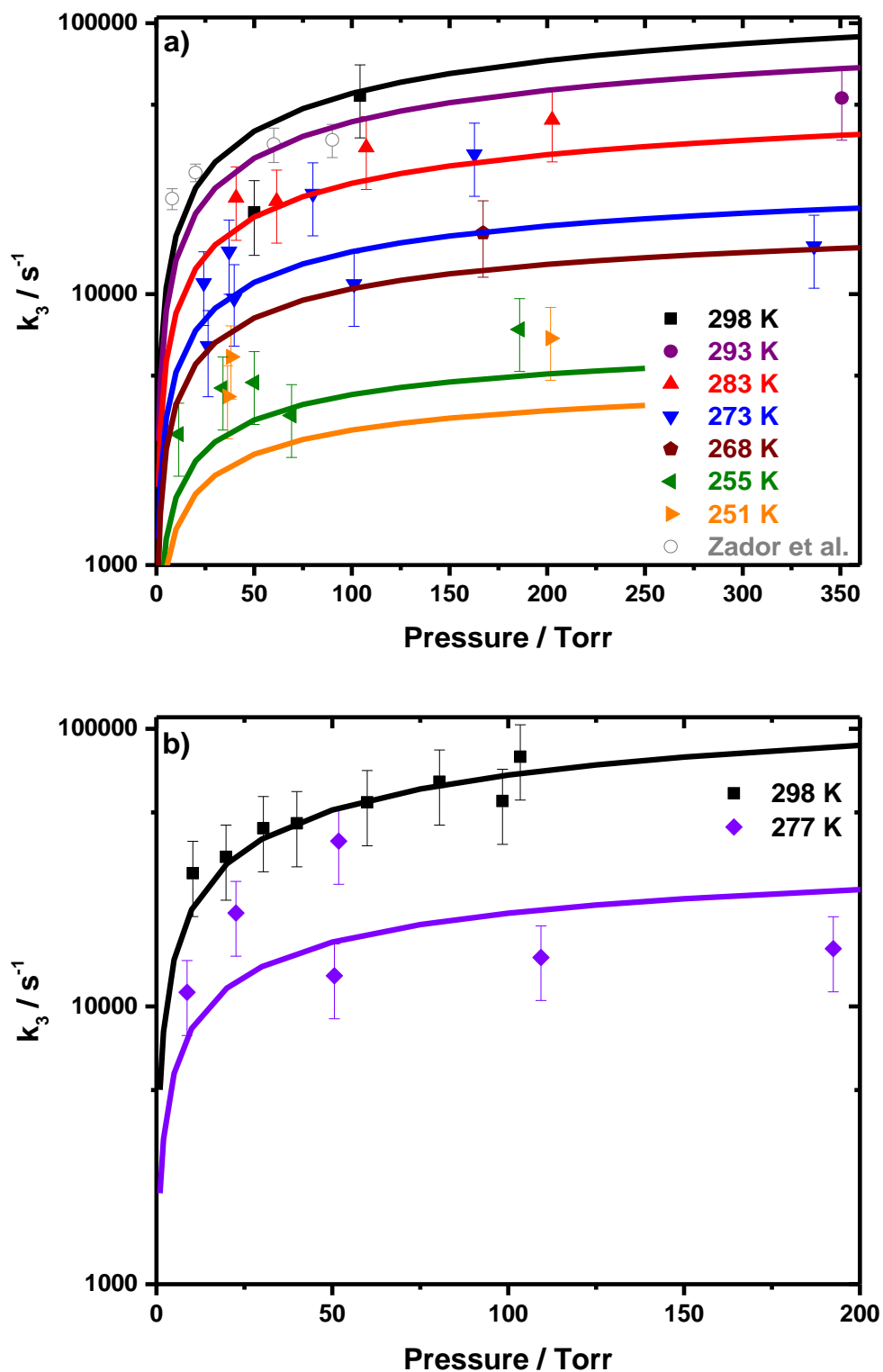


Figure 4: Temperature and pressure dependence of k_3 from 251 – 298 K in a) He bath gas and b) N_2 bath gas. The solid lines are the MESMER fits which give a barrier height to decomposition of 44.7 kJ mol^{-1} , with $\Delta E_{\text{down}} = 89 \text{ cm}^{-1}$ in He and $\Delta E_{\text{down}} = 147 \text{ cm}^{-1}$ in N_2 . Data reported by Zádor et al.⁸ for experiments at $(298 \pm 2) \text{ K}$ in He bath gas are also shown (open circles).

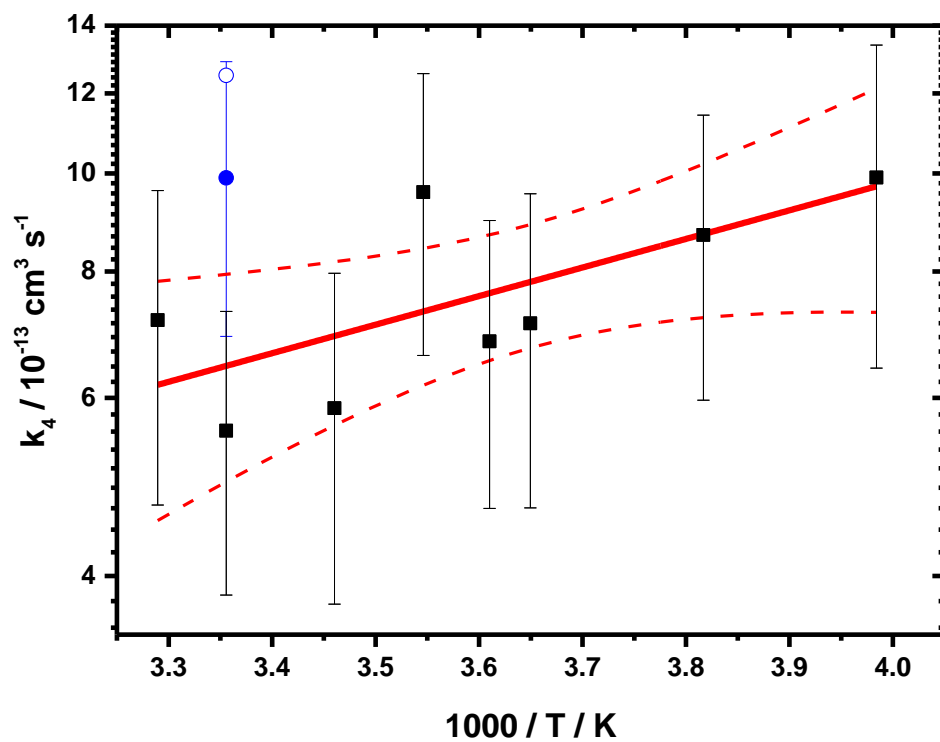


Figure 5: Experimental results for k_4 as a function of temperature (black points) with Arrhenius fit to data (red solid line), giving $A = (7.3 \pm 6.8) \times 10^{-14} \text{ cm}^3 \text{ s}^{-1}$ and $E_a = -(5.4 \pm 2.1) \text{ kJ mol}^{-1}$. Confidence intervals (95 %) for the Arrhenius fit are given by the red broken lines. Also shown are the measured (blue filled circle) and calculated (blue open circle) results for k_4 at room temperature reported by Zádor et al.⁸

Tables

T / K	p / Torr	Bath gas	Photolysis wavelength / nm	k_3 / s^{-1}
298	10	N ₂	248	30200 ± 9100
298	20	N ₂	248	34600 ± 10400
298	30	N ₂	248	43800 ± 13200
298	40	N ₂	248	45600 ± 13800
298	60	N ₂	248	54300 ± 16400
298	80	N ₂	248	64400 ± 19500
298	100	N ₂	248	54900 ± 16600
298	100	N ₂	248	79300 ± 24000
298	50	He	193	20100 ± 6200
298	100	He	193	53900 ± 16200
293	350	He	193	52900 ± 15900
283	40	He	193	22600 ± 6900
283	60	He	193	22100 ± 6600
283	110	He	193	34800 ± 10400
283	200	He	193	44000 ± 13200
277	10	N ₂	193	11200 ± 3400
277	20	N ₂	193	21700 ± 6500
277	50	N ₂	193	12900 ± 3900
277	50	N ₂	193	39400 ± 11900
277	110	N ₂	193	15000 ± 4500
277	190	N ₂	193	16200 ± 4900
273	25	He	193	11000 ± 3300
273	25	He	193	6400 ± 2300
273	40	He	193	14400 ± 4400
273	40	He	193	9600 ± 3200
273	80	He	193	23500 ± 7100
273	100	He	193	10900 ± 3300
273	160	He	193	32800 ± 9900
273	340	He	193	15000 ± 4500
268	170	He	193	16800 ± 5300
255	10	He	193	3000 ± 900
255	35	He	193	4500 ± 1400
255	50	He	193	4700 ± 1400
255	70	He	193	3600 ± 1100
255	185	He	193	7400 ± 2200
251	35	He	193	4200 ± 1300
251	40	He	193	5900 ± 1800
251	200	He	193	6900 ± 2100

Table 1: Summary of results for k_3 .

T / K	$k_4 / 10^{-13} \text{ cm}^3 \text{ s}^{-1}$
304	7.2 ± 2.5
298	5.6 ± 1.7
289	5.9 ± 2.1
282	9.6 ± 3.0
277	6.8 ± 2.2
274	7.1 ± 2.4
262	8.7 ± 2.7
251	9.9 ± 3.5

Table 2: Summary of results for k_4 .

References

- (1) Zador, J.; Taatjes, C. A.; Fernandes, R. X., Kinetics of elementary reactions in low-temperature autoignition chemistry, *Prog. Energy Combust. Sci.* 2011, 37, 371-421.
- (2) Pilling, M. J.; Robertson, S. H.; Seakins, P. W., Elementary radical reactions and autoignition, *J. Chem. Soc. Farad. Trans.* 1995, 91, 23, 4179-4188.
- (3) Praske, E.; Otkjaer, R. V.; Crouse, J. D.; Hethcox, J. C.; Stoltz, B. M.; Kjaergaard, H. G.; Wennberg, P. O., Atmospheric autoxidation is increasingly important in urban and suburban North America, *Proc. Nat. Acad. Sci.* 2018, 115, 64-69.
- (4) Scheer, A. M.; Welz, O.; Zador, J.; Osborn, D. L.; Taatjes, C. A., Low-temperature combustion chemistry of novel biofuels: resonance-stabilized QOOH in the oxidation of diethyl ketone, *Phys. Chem. Chem. Phys.* 2014, 16, 13027-13040.
- (5) Welz, O.; Klippenstein, S. J.; Harding, L. B.; Taatjes, C. A.; Zador, J., Unconventional peroxy chemistry in alcohol oxidation: The water elimination pathway, *J. Phys. Chem. Lett.* 2013, 4, 350-354.
- (6) Koritzke, A. L.; Davis, J. C.; Caravan, R. L.; Christianson, M. G.; Osborn, D. L.; Taatjes, C. A.; Rotavera, B., QOOH-mediated reactions in cyclohexene oxidation, *Proc. Combust. Inst.* 2019, 37, 323-335.
- (7) Savee, J. D.; Papajak, E.; Rotavera, B.; Huang, H. F.; Eskola, A. J.; Welz, O.; Sheps, L.; Taatjes, C. A.; Zador, J.; Osborn, D. L., Direct observation and kinetics of a hydroperoxyalkyl radical (QOOH), *Science* 2015, 347, 643-646.
- (8) Zador, J.; Huang, H. F.; Welz, O.; Zetterberg, J.; Osborn, D. L.; Taatjes, C. A., Directly measuring reaction kinetics of QOOH – a crucial but elusive intermediate in hydrocarbon autoignition, *Phys. Chem. Chem. Phys.* 2013, 15, 10753-10760.
- (9) Baasandorj, M.; Papanastasiou, D. K.; Talukdar, R. K.; Hasson, A. S.; Burkholder, J. B., (CH₃)₃COOH (tert-butyl hydroperoxide): OH reaction rate coefficients between 206 and 375 K and the OH photolysis quantum yield at 248 nm, *Phys. Chem. Chem. Phys.* 2010, 12, 12101-12111.
- (10) Ren, H.; Zhang, L. L.; Wang, R. S.; Pan, X. M., Theoretical studies on the mechanisms and dynamics of OH radical with (CH₃)₃COOH and (CH₃)₂CHOOH, *J. Phys. Chem. A* 2012, 116, 10647-10655.
- (11) Eskola, A. J.; Carr, S. A.; Shannon, R. J.; Wang, B.; Blitz, M. A.; Pilling, M. J.; Seakins, P. W.; Robertson, S. H., Analysis of the kinetics and yields of OH radical production from the CH₃OCH₂ + O₂ reaction in the temperature range 195-650 K: An experimental and computational study, *J. Phys. Chem. A* 2014, 118, 6773-6788.
- (12) Glowacki, D. R.; Liang, C.-H.; Morley, C.; Pilling, M. J.; Robertson, S. H., MESMER: An open-source master equation solver for multi-energy well reactions, *J. Phys. Chem. A* 2012, 116, 9545-9560.

- (13) Glowacki, D. R.; Lockhart, J.; Blitz, M. A.; Klippenstein, S. J.; Pilling, M. J.; Robertson, S. H.; Seakins, P. W., Interception of excited vibrational quantum states by O₂ in atmospheric association reactions, *Science* 2012, 337, 1066-1069.
- (14) Carr, S. A.; Romero, M. T. B.; Blitz, M.; Pilling, M. J.; Heard, D. E.; Seakins, P. W., OH yields from the CH₃CO + O₂ reaction using an internal standard, *Chem. Phys. Lett.* 2007, 445, 108-112.
- (15) Baeza-Romero, M. T.; Glowacki, D. R.; Blitz, M. A.; Heard, D. E.; Pilling, M. J.; Rickard, A. R.; Seakins, P. W., A combined experimental and theoretical study of the reaction between methylglyoxal and OH/OD radical: OH regeneration, *Phys. Chem. Chem. Phys.* 2007, 9, 4114-4128.
- (16) Baklanov, A. V.; Krasnoperov, L. N., Oxalyl chloride – A clean source of chlorine atoms for kinetic studies, *J. Phys. Chem. A* 2001, 105, 97-103.
- (17) Ghosh, B.; Papanastasiou, D. K.; Burkholder, J. B., Oxalyl chloride, ClC(O)C(O)Cl: UV/vis spectrum and Cl atom photolysis quantum yields at 193, 248, and 351 nm, *J. Chem. Phys.* 2012, 137, 164315, 1-12.
- (18) McMillen, D. F.; Golden, D. M., Hydrocarbon bond-dissociation energies, *Ann. Rev. Phys. Chem.* 1982, 33, 493-532.
- (19) Choi, N.; Pilling, M. J.; Seakins, P. W.; Wang, L., Studies of site selective hydrogen atom abstractions by Cl atoms from isobutane and propane by laser flash photolysis/IR diode laser spectroscopy, *Phys. Chem. Chem. Phys.* 2006, 8, 2172-2178.
- (20) Wu, H.; Mu, Y. J.; Zhang, X. S.; Jiang, G. B., Relative rate constants for the reactions of hydroxyl radicals and chlorine atoms with a series of aliphatic alcohols, *Int. J. Chem. Kinet.* 2003, 35, 81-87.
- (21) Frisch, M. J.; Trucks, G. W.; Schlegel, H. B.; Scuseria, G. E.; Robb, M. A.; Cheeseman, J. R.; Scalmani, G.; Barone, V.; Petersson, G. A.; Nakatsuji, H. et al., *Gaussian 09*, Gaussian Inc., Wallingford, CT 2009.
- (22) Shannon, R. J.; Robertson, S. H.; Blitz, M. A.; Seakins, P. W., Bimolecular reactions of activated species: An analysis of problematic HC(O)C(O) chemistry, *Chem. Phys. Lett.* 2016, 661, 58-64.
- (23) Joback, K. G.; Reid, R. C., Estimation of pure-component properties from group-contributions, *Chem. Eng. Commun.* 1987, 57, 233-243.
- (24) Gao, C. W.; Allen, J. W.; Green, W. H.; West, R. H., Reaction mechanism generator: Automatic construction of chemical kinetic mechanisms, *Comp. Phys. Commun.* 2016, 203, 212-225.
- (25) Troe, J.; Ushakov, V.G., Representation of “broad” falloff curves for dissociation and recombination reactions, *Z. Phys. Chem.* 2014, 228, 1, 1-10.
- (26) Lightfoot, P. D.; Cox, R. A.; Crowley, J. N.; Destriau, M.; Hayman, G. D.; Jenkin, M. E.; Moortgat, G. K.; Zabel, F., Organic peroxy radicals – Kinetics, spectroscopy and tropospheric chemistry, *Atmos. Environ. A* 1992, 26, 1805-1961.

- (27) Lenhardt, T. M.; McDade, C. E.; Bayes, K. D., Rates of reaction of butyl radicals with molecular oxygen, *J. Chem. Phys.*, 1980, 72, 304-310.
- (28) Langer, S.; Ljungstrom, E.; Ellermann, T.; Nielsen, O. J.; Sehested, Pulse radiolysis study of reactions of alkyl and alkylperoxy radicals originating from methyl tert-butyl ether in the gas phase, *J. Chem. Phys. Lett.* 1995, 240, 499-505.
- (29) Dilger, H.; Stolmar, M.; TregennaPiggott, P. L. W.; Roduner, E.; Reid, I. D., Gas phase addition kinetics of the tert-butyl radical to oxygen, *Ber. Bunsen-Ges. Phys. Chem. Chem. Phys.* 1997, 101, 956-960.
- (30) Villano, S. M.; Huynh, L. K.; Carstensen, H. H.; Dean, A. M., High pressure rate rules for alkyl + O₂ reactions 1: The dissociation, concerted elimination, and isomerization channels of the alkyl peroxy radical, *J. Phys. Chem. A*, 2011, 115, 13425-13442.

TOC Graphic

